Unitary IPSPs evoked by interneurons at the stratum radiatum–stratum lacunosum-moleculare border in the CA1 area of the rat hippocampus *in vitro*

Imre Vida*†, Katalin Halasy*‡, Csaba Szinyei*, Peter Somogyi* and Eberhard H. Buhl*

**MRC Anatomical Neuropharmacology Unit, Department of Pharmacology, Oxford University, Oxford OX1 3TH, UK, †Institute of Pharmacology, University Medical School of Pécs, H-7643 Pécs, Hungary and ‡Department of Anatomy and Histology, University of Veterinary Science, Budapest, Hungary*

(Received 30 May 1997; accepted after revision 25 September 1997)

1. Hippocampal non-principal neurons at the stratum radiatum–stratum lacunosum-moleculare border (R–LM interneurons) of the CA1 area may constitute several cell classes and have been implicated in the generation of GABAergic unitary IPSPs. Using biocytin-filled electrodes we recorded R–LM interneurons intracellularly *in vitro* and determined their postsynaptic effects in concomitantly recorded pyramidal cells.

2. Light microscopic analysis revealed four populations of R–LM interneurons with distinct axons: (1) basket cells ($n = 4$) with axons predominantly ramifying in the pyramidal cell layer; (2) Schaffer collateral/commissural pathway-associated interneurons ($n = 10$) stratifying in stratum radiatum and, to a lesser extent, stratum oriens; (3) perforant pathway-associated interneurons ($n = 6$) innervating the perforant path termination zone in stratum lacunosum-moleculare of the CA1 area as well as equivalent portions of the dentate gyrus and subiculum; and (4) neurogliaform interneurons ($n = 2$) characterized by their dense, compact axonal and dendritic arbour.

3. Random electron microscopic sampling of synaptic targets revealed a preponderance of pyramidal neurons as postsynaptic elements. Basket cells had a synaptic target preference for somata and proximal dendrites, whereas the remainder of R–LM interneurons innervated dendritic shafts and spines. The axon of dendrite-targeting cells formed up to six putative contacts with individual postsynaptic pyramidal cells.

4. Anatomically recovered R–LM interneurons ($n = 22$) had a mean resting membrane potential of $-56{\cdot}7 \pm 3{\cdot}6$ mV, a membrane time constant of $12{\cdot}9 \pm 7{\cdot}7$ ms and an input resistance of $86{\cdot}4 \pm 29{\cdot}2$ MΩ. Depolarizing current pulses generally elicited overshooting action potentials ($70{\cdot}8 \pm 6{\cdot}9$ mV) which had a mean duration, when measured at half-amplitude, of $0{\cdot}7 \pm 0{\cdot}1$ ms. In response to prolonged (> 200 ms) depolarizing current pulses all R–LM interneurons displayed (a varying degree of) spike frequency adaptation.

5. Basket cells, Schaffer-associated and neurogliaform interneurons elicited small-amplitude (< 2 mV), short-latency IPSPs in postsynaptic pyramids ($n = 5$, 13 and 1, respectively). Those interactions in which an effect was elicited with the repetitive activation of the presynaptic neuron ($n = 13$) showed a substantial degree of postsynaptic response summation. Unitary IPSPs had fast kinetics and, whenever tested ($n = 5$; 1 basket cell and 4 Schaffer-associated interneurons), were abolished by the $GABA_A$ receptor antagonist bicuculline.

6. Thus, R–LM interneurons comprise several distinct populations which evoke fast $GABA_A$ receptor-mediated IPSPs. The domain-specific innervation of postsynaptic pyramidal cells suggests functionally diverse effects on the integration of afferent information in functionally non-equivalent compartments of pyramidal cells.

Hippocampal non-principal neurons which release the amino acid neurotransmitter γ-aminobutyric acid (GABA) are composed of an, as yet, unknown number of distinct classes (Freund & Buzsáki, 1996). Although some of them project to other hippocampal subfields or even to extrahippocampal brain areas (reviewed in Freund & Buzsáki, 1996), non-principal neurons generally give rise to a rich local axon plexus and are, for this reason, referred to as interneurons. The great diversity of GABAergic interneurons is reflected in their complex synaptic circuitry and, perhaps most emphatically, in their efferent connectivity (Somogyi, Freund, Hodgson, Somogyi, Beroukas & Smith, 1985; Gulyás, Miles, Hájos & Freund, 1993; Halasy & Somogyi, 1993; Buhl, Halasy & Somogyi, 1994). In this regard, interneurons may be specific not only in their preference for particular cell classes (Gulyás, Hájos & Freund, 1996; Acsády, Görcs & Freund, 1996; Cobb *et al.* 1997) but also in their selective innervation of spatially segregated membrane compartments on the surface of their postsynaptic targets (Somogyi *et al.* 1985; Halasy, Buhl, Lörinczi, Tamás & Somogyi, 1996). Furthermore, interneuronal axonal arbours in all hippocampal subfields have been shown to co-stratify with major glutamatergic pathways (Gulyás *et al.* 1993; Han, Buhl, Lörinczi & Somogyi, 1993; Buhl *et al.* 1994; Halasy *et al.* 1996), thus providing a substrate for the input-specific modulation of hippocampal afferents.

Extracellular mono- or disynaptic activation of an unidentified, presumably heterogeneous, pool of interneurons typically evokes biphasic $GABA_A$ and $GABA_B$ receptor-mediated inhibitory postsynaptic potentials (IPSPs) in concomitantly recorded neurons (for review see Thompson, 1994). It has been suggested that the fast $GABA_A$ receptor component is prevalent in the perisomatic region, whereas slower $GABA_B$ responses were thought to predominate in the dendritic region (Misgeld, Bijak & Jarolimek, 1995). In view of their well-established domain specificity it is thus conceivable that distinct subsets of interneurons may be involved in the differential activation of spatially segregated GABA receptor populations (Misgeld *et al.* 1995). Indeed, several different experimental protocols, such as the highly focal release of endogenous GABA and microstimulation experiments, have provided evidence, albeit indirect, to support this notion (Solis & Nicoll, 1992; Williams & Lacaille, 1992). In contrast, paired intracellular recording experiments in the hippocampal CA1 area have shown that selective activation of individual GABAergic interneurons, such as basket and axo-axonic cells, does evoke IPSPs which are mediated, perhaps exclusively, through $GABA_A$ receptors (Buhl *et al.* 1994; Buhl, Cobb, Halasy & Somogyi, 1995). These findings have been recently extended by stimulating a range of morphologically unidentified interneurons in a cell-attached configuration and by demonstrating their postsynaptic effects to be entirely mediated by $GABA_A$ receptors (Ouardouz & Lacaille, 1997). It is thus conceivable that unitary IPSPs may only lead to the opening of subsynaptic $GABA_A$ receptors, whereas additional factors, such as the concomitant activation of several presynaptic neurons or the inhibition of GABA uptake mechanisms, may be required to activate $GABA_B$ receptors with a putative peri- or extrasynaptic location (Thompson & Gähwiler 1992; Mody, DeKoninck, Otis & Soltesz, 1994).

Using paired intracellular recordings of non-principal neurons at the stratum radiatum–stratum lacunosum-moleculare border (R–LM interneurons) with postsynaptic pyramidal cells, in conjunction with *post hoc* light and electron microscopic analysis, we have therefore sought to (1) characterize R–LM interneurons with respect to their efferent connectivity, (2) correlate R–LM cell classes with their postsynaptic effect, and (3) study pharmacologically domain-specific postsynaptic receptor mechanisms following the activation of a single presynaptic neuron under near physiological conditions of synaptic release.

METHODS

Slice preparation

Young adult female Wistar rats (> 120 g) were deeply anaesthetized by an intramuscular injection of ketamine (100 mg kg^{-1}) and xylazine (10 mg kg^{-1}). After cessation of all pain reflexes (e.g. noxious tail pinch) the animals were intracardially perfused with 30–50 ml of chilled artificial cerebrospinal fluid (ACSF) which was initially composed of (mM): 252 sucrose, 3·0 KCl, 1·25 NaH_2PO_4, 24 $NaHCO_3$, 2·0 $MgSO_4$, 2·0 $CaCl_2$ and 10 glucose (Buhl *et al.* 1994). Perfused brains were quickly removed and immersed in a beaker with chilled ACSF. With the aid of a vibroslice (Campden Instruments, Loughborough, UK) 400 μm thick slices were cut in the horizontal plane. The hippocampi were dissected free and transferred to a recording chamber where they were maintained at 34–35 °C on a nylon mesh at the interface between oxygenated ACSF and a humidified atmosphere saturated with 95% O_2–5% CO_2. The flow rate was adjusted to ~1·5 ml min^{-1} and the slices were allowed to equilibrate for 30–45 min in sucrose-containing ACSF, before replacing all sucrose with equi-osmolar NaCl (126 mM), leaving other electrolytes unchanged. All drugs were kept as concentrated stocks which were diluted in ACSF and then superfused. The excitatory amino acid blockers 6-cyano-7-nitroquinoxaline-2,3-dione (CNQX) and DL-2-amino-5-phosphonopentanoic acid (AP5) were obtained from Tocris Cookson (Bristol, UK). Bicuculline hydrochloride was purchased from Sigma.

Intracellular recordings and data analysis

Recording electrodes were manufactured from standard wall borosilicate tubing (1·2 mm o.d., 0·69 mm i.d. with inner filament; Clark Electromedical Instruments, Pangbourne, UK) using a Flaming–Brown-type horizontal puller (model P-87, Sutter Instrument, Novato, CA, USA) and filled with either 1·5 M KCH_3SO_4 or occasionally 1·5 M KCl, with both electrolytes containing 2% biocytin (Buhl *et al.* 1994). Pipette resistances generally were in the range of 90–150 MΩ. All recordings from non-principal cells were obtained in the stratum radiatum–stratum lacunosum-moleculare border region of the hippocampal CA1 area. Putative interneurons were identified due to their physiological characteristics, such as short-duration action potentials followed by large amplitude fast after-hyperpolarizing potentials (fAHPs). Those cells were abandoned which were depolarized above −50 mV

membrane potential and which required continued hyperpolarizing bias currents in excess of −0·2 nA to prevent the spontaneous generation of action potentials. Once a stable recording had been obtained, a second microelectrode was advanced into the pyramidal cell layer with a motorized stepper at an angle of 30–40 deg from the vertical. Following the impalement of a second, sufficiently stable neuron with the physiological characteristics of a pyramidal cell (e.g. broader action potentials, depolarizing and/or late hyperpolarizing after-potentials, and spike frequency adaptation) the cells were tested for synaptic coupling by eliciting single or brief bursts of action potentials with depolarizing current pulses (in the range of 0·1–0·7 nA) in the presumed non-principal cell, whilst monitoring the membrane response in the pyramidal neuron, using on-line spike triggered averaging ($n > 32$). No attempt was made to either quantify or characterize further those dual impalements in which no measurable (< 50 μV) synaptic response was detectable. Capacitive coupling was eliminated on-line using a modified Axoprobe amplifier (Axon Instruments) which was operated in bridge mode. Experimental data were acquired with a PCM-701ES instrumentation recorder (Intracel, Shepreth, UK) and stored on videotapes or using a DTR-1402 digital tape recorder (Biologic, Claix, France). Data analysis was continued off-line by low-pass filtering the data at 1–2 kHz and (re)digitizing the data at 5–10 kHz using commercially available 12 bit A/D boards (RC Electronics Computerscope, Santa Barbara, CA, USA and National Instruments Labmaster +, Newbury, UK) in conjunction with Axograph (Axon Instruments), RC Electronics Computerscope (RC Electronics) and WCP (courtesy of Dr J. Dempster, University of Strathclyde, UK) software packages. Unless indicated otherwise data are expressed as means ± S.D.

Resting membrane potentials were determined following electrode withdrawal and are given as the difference between surface DC potential and the steady-state membrane potential without bias current. Membrane time constants were obtained by fitting a single exponential to small-amplitude hyperpolarizing current pulses (< 0·1 nA). Input resistances were determined from measuring the maximal voltage deflection of 200 ms duration averaged −0·1 nA hyperpolarizing current pulses. Action potential amplitudes were measured from baseline to peak and their duration was determined at half-amplitude. The amplitudes of fAHPs were determined from the shoulder of the preceding action potentials. Unitary IPSP response reversal was estimated by fitting least square regression lines to the mean IPSP amplitudes which had been obtained at several different membrane potentials. For IPSP amplitude measurements the voltage traces of postsynaptic pyramidal cells were averaged over each of four equal-length periods, with those used for noise and IPSP measurements separated by equal intervals. Average voltages for the first two periods preceding the synaptic event were calculated for each sweep and their respective differences provided the noise sample distribution. Likewise, IPSP peak amplitude measurements were obtained from the set of differences between the average voltage of a period preceding the EPSP and the time window encompassing the peak of the IPSP. Data were used only from epochs of recording when the postsynaptic responses remained stationary, defined as epochs during which the mean amplitude running averages remained within ±1 S.D. of the mean amplitude of the first fifty IPSPs within the epoch.

Histological processing and anatomical evaluation

Depolarizing current pulses employed during the recordings in conjunction with intracellular diffusion of biocytin from the electrode resulted in adequate filling of the recorded neurons. After withdrawing the recording electrode, slices were sandwiched between two Millipore filters and fixed in 2·5% paraformaldehyde, 1·25% glutaraldehyde and 15% (v/v) picric acid in 0·1 M phosphate buffer (PB; pH 7·4), usually overnight. Following gelatine re-embedding, taking care to keep them flat, slices were re-sectioned on a vibratome at 50–60 μm thickness and processed for light and electron microscopy using the avidin-biotinylated horseradish peroxidase complex (ABC; Vector Laboratories, Peterborough, UK), in accordance with previously described procedures (Han *et al.* 1993; Buhl *et al.* 1994). After their embedding in epoxy resin all recovered interneurons with extensive axonal filling were scrutinized in the light microscope to establish preliminary classification according to their salient morphological features (see Results). In several instances (see Figs 1–3), both pre- and postsynaptic cells were completely reconstructed from serial 60 μm sections using a light microscope and drawing tube at × 1000–1250 magnification. Alternatively, when no postsynaptic pyramidal cell had been recovered, only the presynaptic interneuron was drawn. In most remaining cases, only the interneuronal dendritic arbours were reconstructed (Fig. 7). On five occasions (Figs 2 and 3) all putative sites of synaptic interaction between pre- and postsynaptic neuron were mapped in the light microscope. Subsequent to light microscopic analysis, representative axon-rich areas, including all layers covered by the axonal field, were re-embedded for ultrathin sectioning. Serial sections were cut and mounted on single-slot Formvar-coated (TAAB, Reading, UK) copper grids and contrasted with lead citrate. The sections were scanned in the electron microscope and all biocytin-filled axonal profiles were followed until they formed synaptic contacts. Although occasionally the identification of postsynaptic specializations proved to be impossible due to the electron-opaque reaction end product or the degeneration of the postsynaptic element, we verified synaptic junctions based on the following criteria: (1) vesicle accumulation in the presynaptic axonal varicosity, and (2) rigid membrane apposition between the pre- and postsynaptic element with a characteristic widening of the extracellular space. Since all labelled boutons were followed and the plane of the section randomly cut through the axonal branches, the above procedure ensured a random sample of postsynaptic targets. Each presynaptic terminal that was studied was completely examined in serial sections to establish the number of synapses it formed. Tracing of serial sections was also useful to distinguish between dendritic spines and small calibre dendritic shafts as postsynaptic elements. In some cases, when the tracing was not feasible, small diameter postsynaptic profiles containing mitochondria and/or microtubules were classified as dendritic shafts. Regarding the origin of dendritic shafts, those exhibiting features such as prominent dendritic varicosities, the overall absence of dendritic spines and, importantly, converging asymmetrical synaptic input were categorized as interneuron dendrites. Thus, for a total of fourteen presynaptic cells, comprising all light microscopically established categories, a minimum of ten synaptic contacts were rigorously identified.

RESULTS

During the recordings R–LM interneurons were identified primarily by virtue of their position, but also on the basis of their short-duration action potentials, which were generally followed by a fAHP (Table 1). On physiological grounds, R–LM interneurons were clearly distinguishable from dendritic recordings of pyramidal cells and were also different from somatic recordings of pyramidal cells, which are occasionally encountered in the upper part of stratum

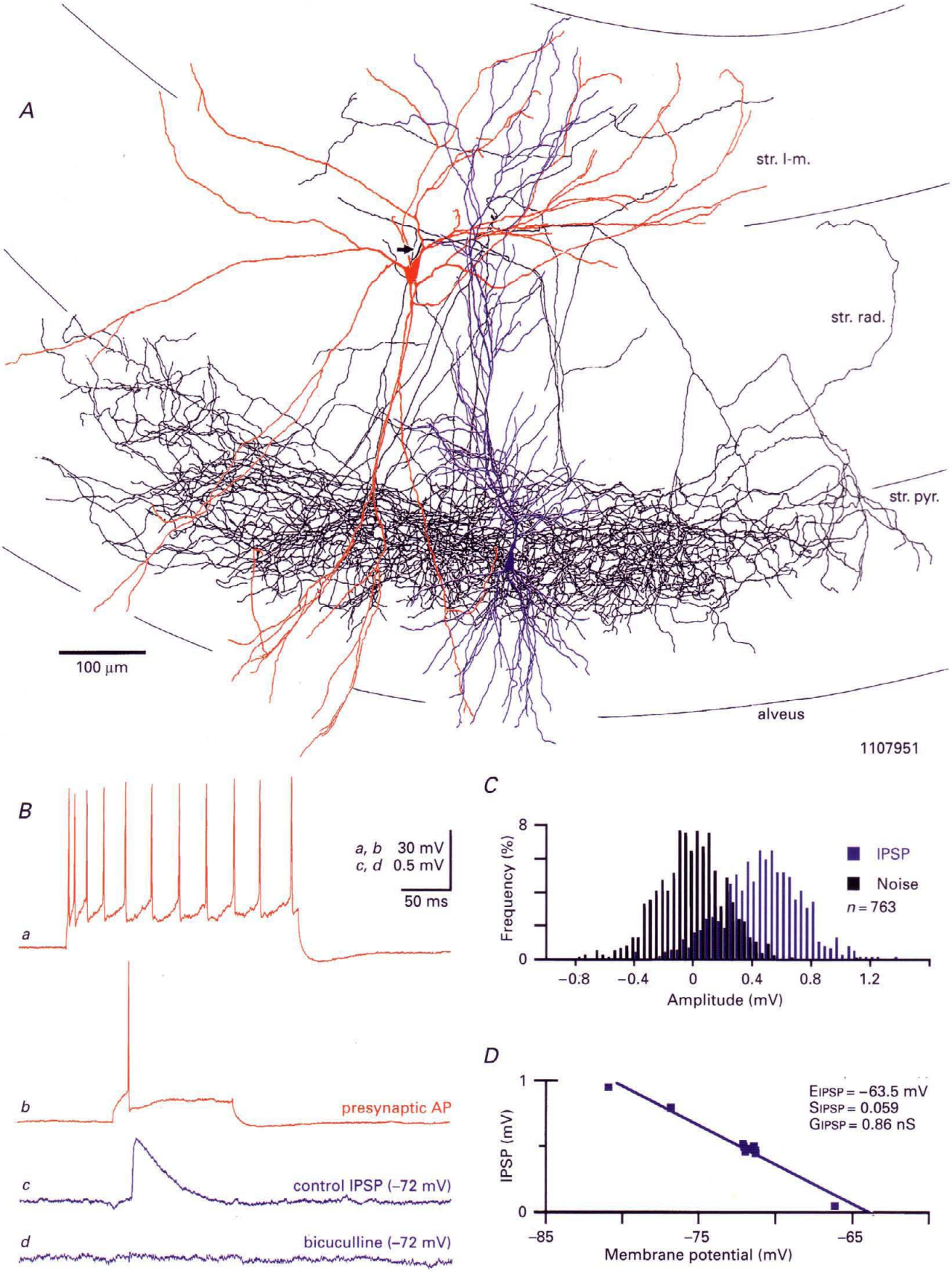

Figure. 1. For legend see facing page.

Table 1. Intrinsic physiological properties and postsynaptic effects of R–LM interneurons

R–LM cell type	Membrane potential (mV)	Input resistance (MΩ)	Time constant (ms)	Action pot. amplitude (mV)	Action pot. duration (ms)	fAHP (ms)	Coupling ratio* (%)	Single action potential-evoked IPSP amplitude† (mV)
Basket ($n = 4$)	−60·0 ± 5·2 (−53/−64)	70·6 ± 18·9 (48/94)	9·2 ± 6·0 (4·2/17·4)	75·7 ± 6·2 (70·6/84·6)	0·67 ± 0·2 (0·45/0·93)	−7·2 ± 1·6 (−5·8/−9·4)	83 (5/6) (0·50/0·56)	0·53 ± 0·04 (2)
Schaffer-associated ($n = 10$)	−55·8 ± 2·8 (−50/−59)	96·3 ± 36·0 (53/180)	16·2 ± 8·9 (7·5/38·1)	70·8 ± 8·0 (58·7/78·5)	0·74 ± 0·1 (0·55/0·90)	−11·4 ± 2·8 (−5·2/−15·4)	65 (13/20) (0·07/0·08)	0·07 ± 0·01 (3)
Perforated path-associated ($n = 6$)	−55·4 ± 3·1 (−51/−60)	84·2 ± 23·7 (65/127)	11·9 ± 5·9 (4·3/22·0)	69·4 ± 5·3 (63·0/78·2)	0·73 ± 0·1 (0·53/0·90)	−7·0 ± 2·6 (−3·6/−9·7)	0 (0/20)	n.a.
Neurogliaform ($n = 2$)	−58·3 ± 2·4 (−57/−60)	74·7 ± 6·0 (70/79)	6·5 ± 0·1 (6·4/6·6)	65·1 ± 0·4 (64·9/65·4)	0·80 ± 0·1 (0·75/0·84)	−10·8 ± 1·4 (−9·8/−11·8)	33 (1/3)	0·30 (1)
All interneurons ($n = 22$)	−56·7 ± 3·6 (−50/−64)	86·4 ± 29·2 (48/180)	12·9 ± 7·7 (4·2/38·1)	70·8 ± 6·9 (58·7/84·6)	0·73 ± 0·1 (0·45/0·93)	−9·4 ± 3·2 (−3·6/−15·4)	39 (19/49)	
Postsynaptic pyramidal cells ($n = 19$)	−59·9 ± 2·5 (−56/−65)	52·3 ± 10·8 (34/74)	16·2 ± 4·1 (8·2/24·7)	78·8 ± 11·7 (65·1/107·1)	1·15 ± 0·2 (0·90/1·88)	−4·7 ± 2·0 (−1·8/−8·3)		

Data show the means and range (min./max.). * Coupling ratio defined as ratio of pyramidal cells tested and pyramidal cells in which a postsynaptic response was detected. † Values of n shown in parentheses.

radiatum (data not shown). Thus, stable intracellular recordings (30 min to 3 h) not requiring the injection of a hyperpolarizing bias current were obtained from twenty-six physiologically identified R–LM interneurons within the hippocampal CA1 area. In four instances, *post hoc* anatomical analysis revealed that the degree of axonal filling was incomplete, leading to their exclusion from further analysis, whereas the remaining twenty-two interneurons showed extensive axonal labelling, presumably comprising most of their arborization which had not been lost during the slicing procedure. However, despite the inevitable loss of some truncated processes the degree of labelling could be very extensive, with several of the axonal trees spreading well beyond the confines of the CA1 area. Our light microscopic reconstructions may thus show a representative approximation of their intact architecture. Indeed, recent quantitative estimates are in support of this notion, demonstrating that in excess of 50% of the axonal arbour of CA1 cell body layer interneurons is contained within the confines of a 400 μm thick *in vitro* slice preparation (Halasy *et al.* 1996).

Figure 1. Synaptically connected basket-to-pyramidal cell pair in the CA1 area of the rat hippocampus

A, light microscopic reconstruction of the basket cell at the stratum radiatum–stratum lacunosum-moleculare border (soma and dendrites in red, axon in black; basket cell main axon denoted by arrow) and the synaptically coupled pyramidal cell (soma and dendrites in blue, spines and axon not shown). *Ba*, injection of a depolarizing current pulse (200 ms duration, 0·7 nA amplitude) into the basket cell elicited a train of accommodating action potentials. *Bb*, single basket cell action potentials evoked by depolarizing current pulses (0·25 nA) elicited short-latency, fast IPSPs in the concomitantly recorded pyramidal cell (*Bc*; average of 763 sweeps). Unitary IPSPs were hyperpolarizing events due to chloride loading of the pyramidal cell. The postsynaptic response was completely abolished by 10 μM of the bath applied $GABA_A$ receptor antagonist bicuculline (*Bd*; average of 275 sweeps). *C*, amplitude histogram of unitary IPSPs (blue; $n = 763$) elicited at an average membrane potential of −71·6 ± 0·6 mV (mean ± S.D.). The corresponding noise distribution (black bars) was determined from the pre-event baseline. *D*, unitary IPSP amplitudes plotted as a function of the pyramidal cell membrane potential. Squares represent average amplitudes of 120–200 successive unitary IPSPs elicited at a given membrane potential. Linear regression was employed to extrapolate the IPSP response reversal (E_{IPSP}) and the resulting slope measurements (S_{IPSP}) were taken to calculate the unitary IPSP conductance (G_{IPSP}). Abbreviations: str. pyr., stratum pyramidale; str. rad, stratum radiatum; str. l-m., stratum lacunosum-moleculare.

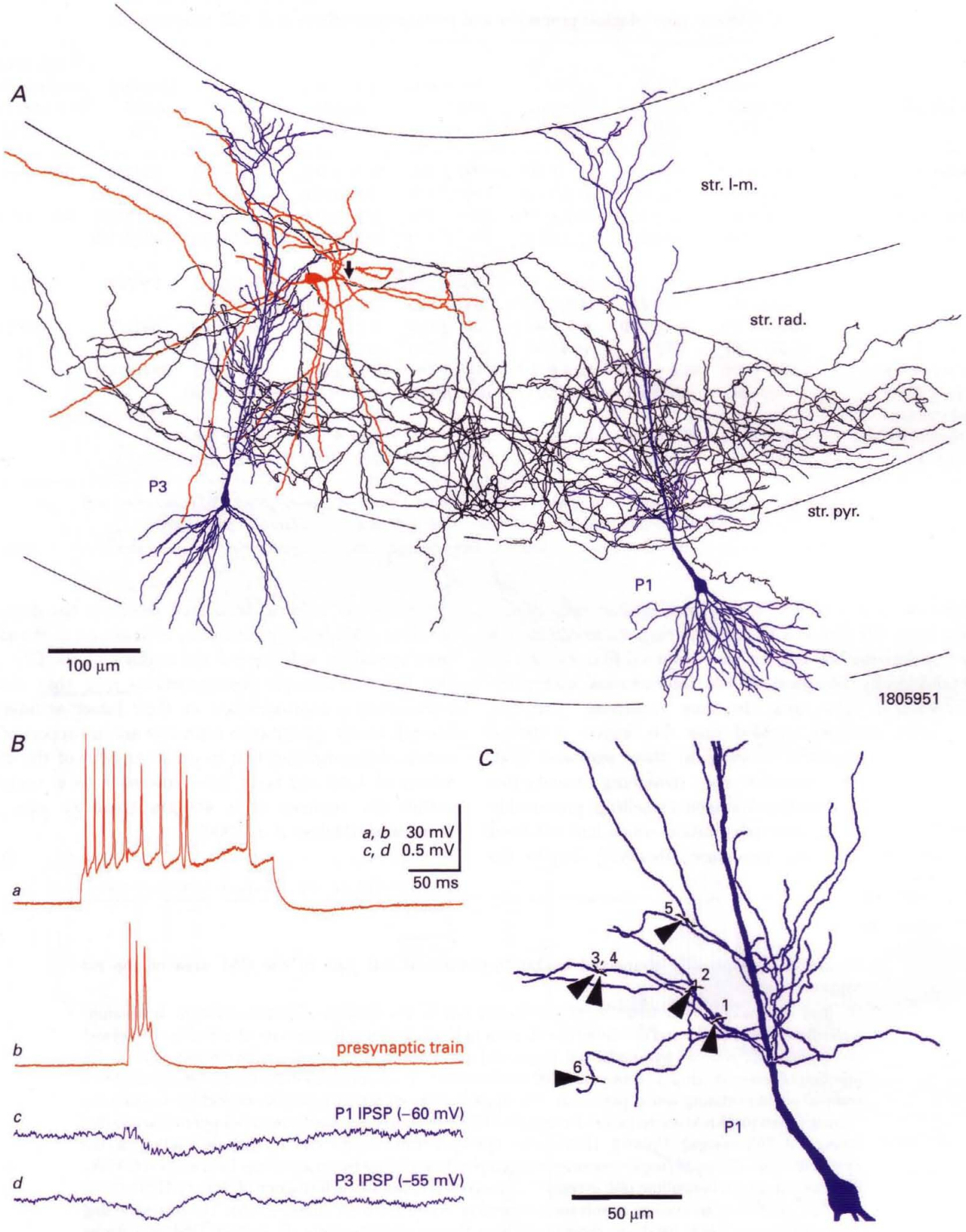

Figure 2. A Schaffer-associated interneuron at the stratum radiatum–stratum lacunosum-moleculare border and two synaptically coupled pyramidal cells

A, light microscopic reconstruction of the biocytin labelled interneuron (soma and dendrites in red, axon in black; main axonal trunk denoted by arrow) and both postsynaptic pyramidal cells (P1 and P3; somata and dendrites in blue, spines and axons omitted). *Ba*, train of accommodating action potentials in response to a

Membrane and firing properties of R–LM interneurons

In view of previously published data (Lacaille & Schwartzkroin, 1988*a*; Williams, Samulack, Beaulieu & Lacaille, 1994), the intrinsic electrophysiological properties of R–LM interneurons were not quantitatively assessed. Only a limited number of parameters were routinely obtained to determine their viability and to account for any significant heterogeneities following their *post hoc* anatomical classification (Table 1). In brief, those R–LM interneurons with (near) complete anatomical recovery ($n = 22$) had an average resting membrane potential of $-56{\cdot}7 \pm 3{\cdot}6$ mV, with a mean membrane time constant of $12{\cdot}9 \pm 7{\cdot}7$ ms and an input resistance of $86{\cdot}4 \pm 29{\cdot}2$ MΩ. Depolarizing current pulses generally elicited overshooting action potentials ($70{\cdot}8 \pm 6{\cdot}9$ mV) which had a duration, when measured at half-amplitude, of $0{\cdot}7 \pm 0{\cdot}1$ ms, the latter two parameters being clearly different from several distinct classes of pyramidal cell layer interneurons which tend to have much briefer, non-overshooting action potentials (Buhl, Szilágyi, Halasy & Somogyi 1996). In response to prolonged (> 200 ms) depolarizing current pulses, all R–LM interneurons displayed spike frequency adaptation, albeit to a varying extent (Figs 1*Ba*, 2*Ba*, 3*Ba*, 4*Aa* and *Ba*, 5*B* and 6*Ba*). In approximately half ($n = 8$) of the cells tested the degree of adaptation was in excess of 80% of the initial firing rate, the latter here defined as the reciprocal of the first interspike interval at or near maximal discharge frequency (~200–300 Hz). In the remainder of cells, spike frequency adaptation was less prominent, which appeared to be largely due to their lower maximal firing rates, whereas steady-state discharge levels (~40–50 Hz) of strongly and weakly adapting cells were relatively similar. Such depolarization-evoked tetanic firing was frequently followed by a long-duration after-hyperpolarization ($n = 13$; Figs 1*Ba*, 3*Ba*, 4*Aa* and *Ba* and 5*B*).

Despite being heterogeneous with regard to their morphological properties (see below), R–LM interneurons as such showed no striking differences which would have justified their categorization solely based on their membrane and firing properties. Interestingly, when grouping interneurons based on their efferent connectivity, appreciable differences became apparent for two of the parameters, membrane time constant and input resistance (Table 1). However, it is conceivable that the use of sharp microelectrodes may have affected these measurements to a differential degree. In addition, the relatively large degree of variability within categories and the small numbers of cells in two of the groups (basket and neurogliaform cells) stress the need for more detailed work using, for example, whole cell recording techniques to ascertain whether these differences can be substantiated.

Light and electron microscopic classification of R–LM interneurons

Light microscopic examination revealed that those R–LM interneurons with extensive dendritic and axonal labelling ($n = 22$) could be incorporated into at least four distinct, non-overlapping categories. Prominent differences were apparent with regard to the lamination pattern of the axon, innervating circumscribed hippocampal layers and/or showing a highly distinct arborization pattern. In those instances, when the axon appeared to be co-laminated with a major glutamatergic hippocampal afferent pathway, such as the perforant pathway, we have followed the terminology originally proposed for dentate gyrus local-circuit neurons (Han *et al.* 1993), which has found relatively widespread acceptance and has been extended to other hippocampal subfields (for review see Freund & Buzsáki, 1996).

(1) The axon of R–LM basket cells ($n = 4$) was confined to the somatic region and adjoining parts of strata radiatum and oriens (Fig. 1*A*). (2) The most abundant type of interneuron, the Schaffer collateral/commissural pathway-associated interneurons ($n = 10$), for reasons of brevity referred to as Schaffer-associated interneurons, predominantly innervated stratum radiatum and, to a lesser extent, stratum oriens (Figs 2*A* and 3*A*). (3) The axon of perforant path-associated interneurons ($n = 6$) was concentrated in stratum lacunosum-moleculare of the CA1 area and could also extend into the molecular layer of both dentate gyrus and subiculum (Fig. 5*A*). (4) The remaining class of local-circuit neuron had a very small stellate dendritic tree and an equally compact axonal arbour within strata radiatum and lacunosum-moleculare (Figs 6*A* and 7). Based on their striking resemblance to a class of previously described neocortical non-principal cells (Szentágothai, 1973) we have thus adopted the term neurogliaform interneurons ($n = 2$).

Regarding the efferent connectivity of hippocampal interneurons, the laminar distribution of axonal arbours is already a reasonably good predictor for their postsynaptic domain specificity (Gulyás *et al.* 1993; Halasy & Somogyi, 1993). However, light microscopic predictions are nevertheless insufficient to assess adequately the post-

depolarizing current pulse (200 ms duration, 0·5 nA amplitude). *Bb*, brief bursts of action potentials in the presynaptic interneuron elicited small-amplitude summated IPSPs in both pyramidal cells (*Bc* and *Bd*; averages of 304 and 479 sweeps, respectively). *C*, light microscopically determined putative sites of synaptic interaction between the interneuron axon (black) and one of the pyramidal cells (P1, blue). All suspect sites (arrowheads, 1–6) were positioned on the shaft of small-calibre dendritic branches. Abbreviations: str. pyr., stratum pyramidale; str. rad., stratum radiatum; str. l-m., stratum lacunosum-moleculare.

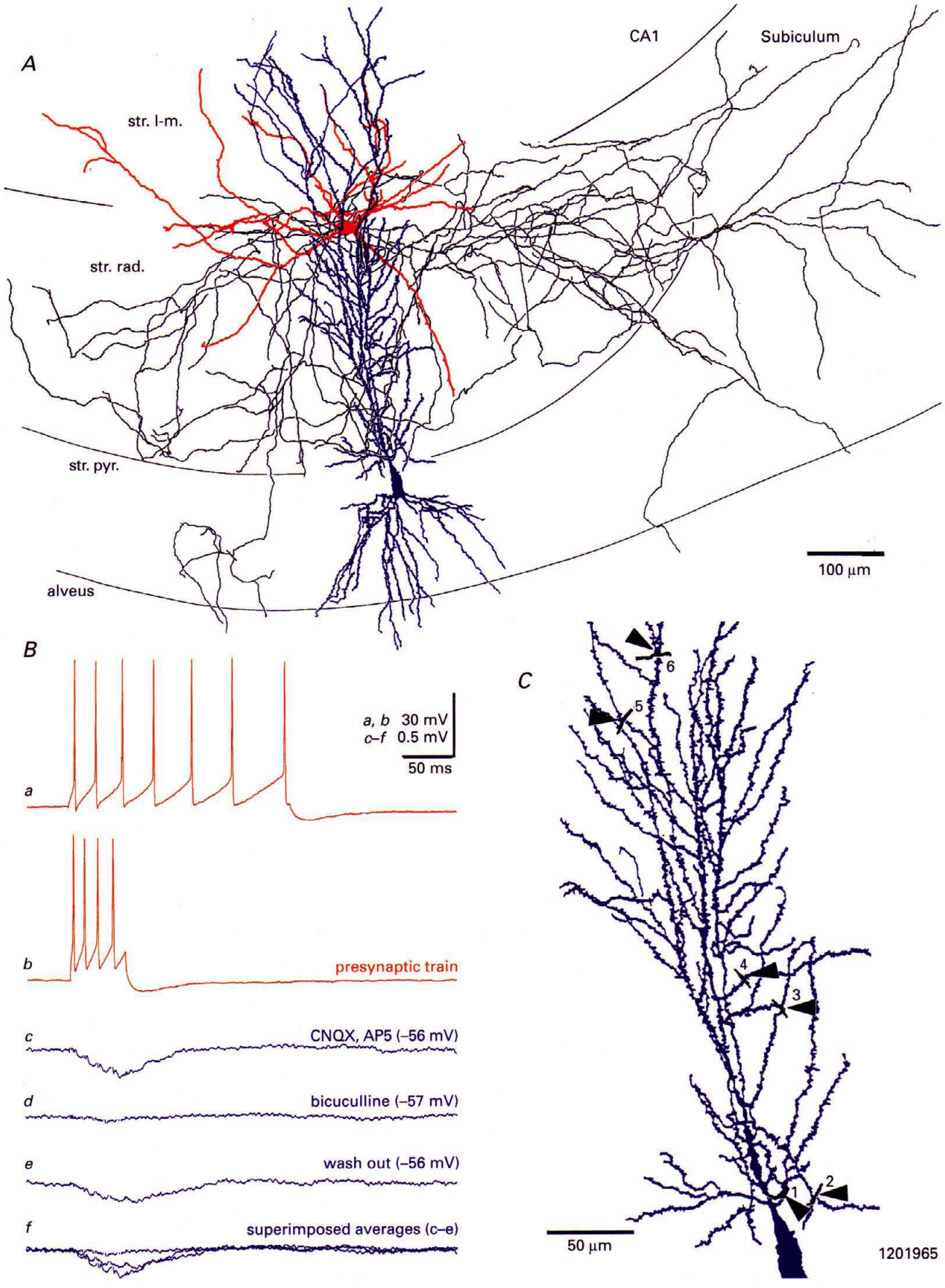

Figure 3. For legend see facing page.

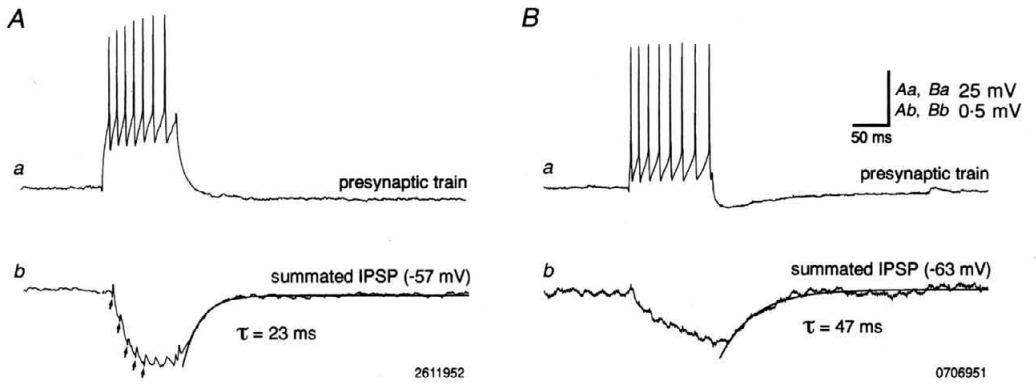

Figure 4. Summation and decay of unitary IPSPs mediated by Schaffer-associated interneurons

Aa, presynaptic trains of 7 action potentials evoked in an interneuron (single sweep) elicited short-latency IPSPs in a simultaneously recorded pyramidal cell (*Ab*; average of 334 sweeps). Initially several postsynaptic responses show a substantial degree of response summation (coupling artifacts denoted by arrows) until a plateau is reached. The IPSP decay could be adequately fitted with a single exponential. *Ba*, similar to the example shown in *A*, tetanic activation of a different Schaffer-associated interneuron (single sweep) elicited incrementally summating IPSPs in a concomitantly recorded pyramidal cell (*Bb*, average of 110 postsynaptic responses). As in panel *Ab* the IPSP decayed monoexponentially.

synaptic target preference for particular membrane domains which may overlap within a given lamina, such as, for example, somata, dendrites and axon initial segments being co-distributed within the pyramidal cell layer. Within the strata radiatum and lacunosum-moleculare potential postsynaptic targets include pyramidal dendrites and spines, the somata of occasional pyramidal cells and the entire somato-dendritic surface of other interneurons. We therefore studied the postsynaptic target distribution of a representative sample of R–LM interneurons ($n = 14$; Table 2), using random electron microscopic sampling of vesicle-containing axonal boutons ($n = 231$), 164 of which were found to establish a total of 170 synaptic junctions (Fig. 8*A–K*; Table 2). Overall, these data indicate that postsynaptic target profiles are relatively stereotyped within the respective groups (see below), notwithstanding some degree of variability, which may be partially due to the limited sample size (10–17 synaptic junctions per cell). Importantly, all cells appeared to favour pyramidal cells as their postsynaptic targets and it is therefore highly probable that none of the cell classes described below overlaps with those categories of R–LM interneurons which have been recently shown to target predominantly, if not exclusively, other interneurons (Gulyás *et al.* 1996; Acsády *et al.* 1996).

Classes of R–LM interneurons

Basket cells. The most salient feature of basket cells ($n = 4$) was their dense terminal axonal arbour which was largely contained within the pyramidal cell layer and, to some extent also, in adjoining parts of the neighbouring strata (Fig. 1*A*). Their characteristic axonal distribution pattern was also reflected in their efferent target profile. Using random electron microscopic sampling techniques, all basket cells could be shown to innervate pyramidal cell somata and

Figure 3. Unitary IPSPs evoked by Schaffer-associated interneurons are mediated by $GABA_A$ receptors

A, light microscopic reconstruction of a representative member of this interneuron class (soma and dendrites in red, axon in black) with a synaptically coupled pyramidal cell (soma and dendrites in blue, axon not shown). *Ba*, accommodating train of action potentials in response to injecting a depolarizing current pulse (200 ms duration; 0·3 nA amplitude) into the interneuron. Brief trains of 4–5 presynaptic action potentials (*Bb* – single sweep) elicited incrementally summating IPSPs in the pyramidal cell. *Bc*, the postsynaptic response remained unaltered in the presence of bath applied glutamate receptor antagonists (10 μM CNQX and 50 μM AP5) but was virtually eliminated due to the successive application of the $GABA_A$ receptor antagonist bicuculline (*Bd*; 10 μM). *Be*, following a 20 min wash-out with bicuculline-free ACSF partial response recovery became apparent, with the unitary IPSP amplitude returning to ~70% of control levels. *Bf*, superimposition of averages shown in *c-e*. *C*, graphic reconstruction showing all 6 light microscopically determined sites of presumed synaptic interaction (arrowheads, 1–6) between the interneuron axon (in black; only partially displayed) and the postsynaptic pyramidal cell (in blue). Abbreviations: str. pyr., stratum pyramidale; str. rad., stratum radiatum; str. l-m., stratum lacunosum-moleculare.

proximal dendrites in approximately equal proportions, whereas they avoided axon initial segments (Table 2 and Fig. 8*A*). A light microscopic reconstruction of a representative example is shown in Fig. 1*A*. This basket cell (1107951; cell 2 of Table 2) gave rise to a single main axon which originated from the soma and ran parallel with the border of stratum lacunosum-moleculare, giving off several collateral branches. These descended towards stratum pyramidale, there forming a dense cloud of terminal axon which had a proximo-distal extent of nearly 1 mm, thus covering most of the CA1 area within the transverse plane. Light microscopic examination of the entire basket cell axon yielded a total bouton number of 7964. Basket cell synaptic terminals formed, on average, slightly in excess of one synapse per bouton (Table 2). This basket cell therefore established ~8000 synaptic junctions within the confines of the slice. It is reasonable to assume that the number of postsynaptic neurons is at least an order of magnitude lower, since the basket cell axon was observed to form multiple sites ($n = 25$) of light microscopically detected appositions of boutons with the labelled postsynaptic pyramidal cell.

With respect to their dendritic architecture, only three of the basket cells showed similarities (Fig. 7). Their dendritic arbours had a bitufted appearance, having branches which spanned all layers of the CA1 region. Compared with

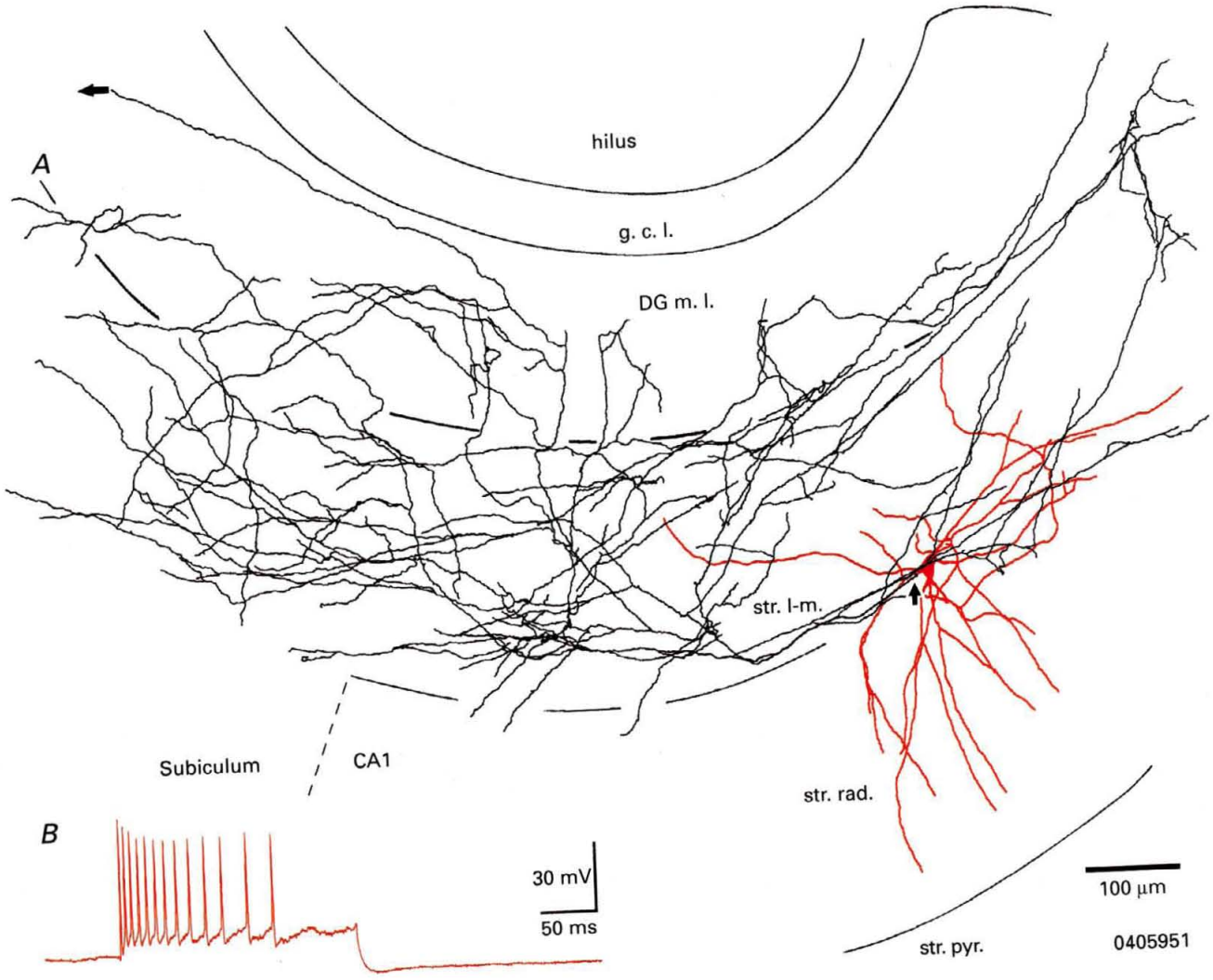

Figure 5. Properties of a perforant path-associated interneuron

A, light microscopic reconstruction of the interneuron (soma and dendrites in red, axon in black, main axon denoted by short arrow) having an axonal arbour not only within stratum lacunosum-moleculare (str. l-m.), but also in the outer portions of the dentate gyrus molecular layer (DG m.l.) and adjoining parts of the subiculum (CA1–subicular border denoted by stippled line). A long arrow denotes the position of an additional collateral which (re)crossed the hippocampal fissure and gave rise to a large axonal plexus in the presubiculum (not shown). *B*, firing pattern of the perforant path-associated interneuron in response to a 200 ms duration 0·7 nA depolarizing current pulse. The cell displayed prominent spike frequency accommodation and a slow after-hyperpolarizing potential. Abbreviations: str. pyr., stratum pyramidale; str. rad., stratum radiatum; g.c.l., granule cell layer; hilus, hilar region of dentate gyrus.

Table 2. Postsynaptic target distribution of interneurons at the stratum radiatum–stratum lacunosum-moleculare border

	Cell	R–LM cell type	Boutons examined	Synaptic boutons	Synaptic junctions	Postsynaptic targets (%)			Unidentified targets (*n*)
						Soma	Dendrite	Spine	
1	1406951	Basket	15	11	12	42	58	0	0
2	1107951	Basket	11	10	11	45	55	0	0
3	1606952	Basket	13	13	13	38·5	61·5	0	0
4	2806951	Basket	12	9	10	55	45	0	1
5	1805951	Schaffer-associated	12	10	10	0	100	0	0
6	1201965	Schaffer-associated	18	15	17	0	100	0	1
7	1212954	Schaffer-associated	10	10	10	0	80	20	0
8	1306951	Schaffer-associated	13	13	13	0	100	0	1
9	2611952	Schaffer-associated	18	16	17	12	88	0	0
10	0405951	Perforant path-associated	27	10	10	0	86	14	3
11	2706951	Perforant path-associated	10	10	10	0	100	0	0
12	1505951	Perforant path-associated	12	10	10	0	90	10	0
13	2606951	Neurogliaform	25	10	10	0	100	0	1
14	0107951	Neurogliaform	35	17	17	0	82	18	0
		Total	231	164	170				

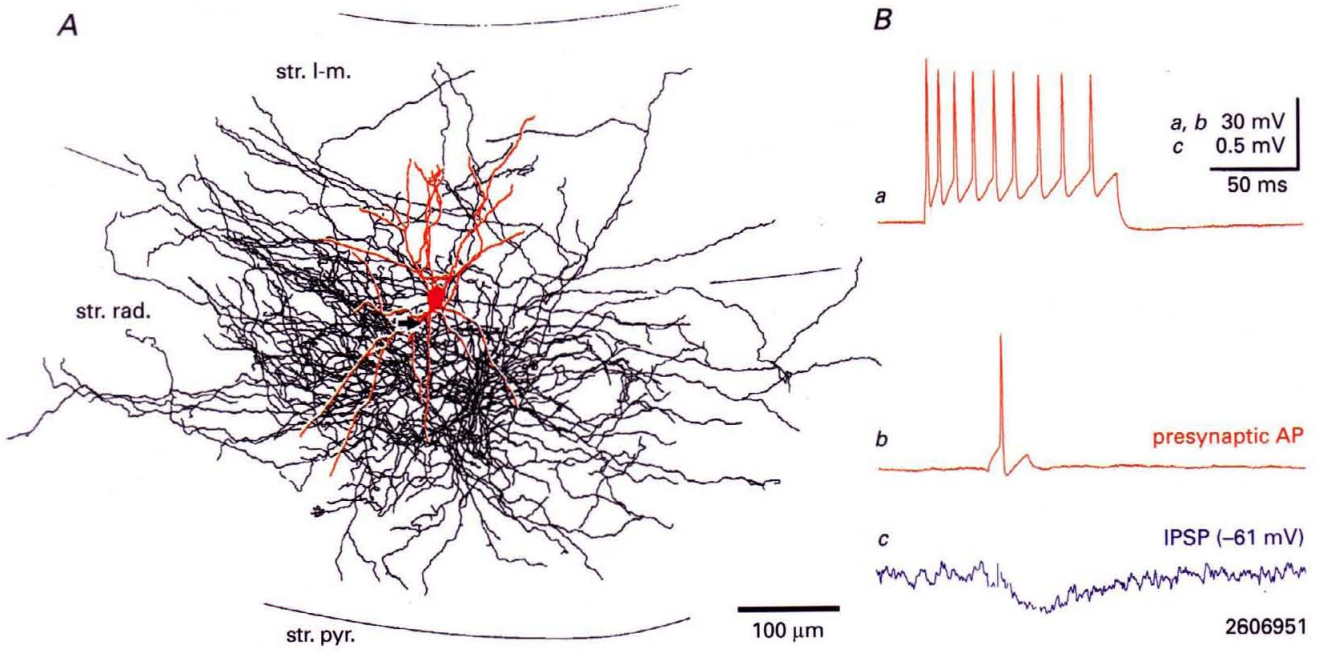

Figure 6. Anatomy and postsynaptic effect of a neurogliaform interneuron at the stratum radiatum–stratum lacunosum-moleculare border

A, light microscopic reconstruction of the interneuron (soma and dendrites in red, axon in black, main axon denoted by arrow). *Ba*, a train of weakly accommodating action potentials evoked by a depolarizing current pulse (100 ms duration; 0·5 nA amplitude) in the neurogliaform interneuron. *Bb*, single action potentials in the presynaptic interneuron elicited small-amplitude fast IPSPs in a simultaneously recorded pyramidal cell (*Bc*; average of 140 sweeps). Due to the brief recording time the pyramidal cell was morphologically not recovered. Abbreviations: str. pyr., stratum pyramidale; str. rad., stratum radiatum; str. l-m., stratum lacunosum-moleculare.

stratum pyramidale basket cells (Halasy *et al.* 1996), their counterparts in the dendritic layers have a higher proportion of their dendrites in stratum lacunosum-moleculare, indicating a more significant role for the entorhinal input in their activation. The dendrites of R–LM basket cell were beaded and predominantly smooth, bearing the occasional spine. These features were somewhat at variance with the appearance of the fourth basket cell (2806951; cell 4 of Table 2). This neuron also had a large dendritic tuft in stratum lacunosum-moleculare, but was nearly devoid of dendrites in the other layers (Fig. 7). Moreover, since the dendrites of this neuron were also appreciably more spiny, we cannot, at present, exclude the possibility that R–LM basket cells may be composed of more than one distinct neuronal class.

Schaffer-associated interneurons. Although this class of interneuron had axonal arbours which were predominantly located in stratum radiatum (Figs 2*A* and 3*A*; $n = 10$), collaterals were often found to traverse the pyramidal cell layer and arborize in stratum oriens (Fig. 3*A*). As an additional characteristic of this type of R–LM interneuron, major axons frequently emerged from a proximal dendrite and ran parallel to the stratum radiatum–stratum lacunosum-moleculare border, giving off descending branches. The axonal terminal field of the cell illustrated in Fig. 2*A* (1805951; cell 5 of Table 2) had a proximo-distal extent of ~1·1 mm and contained a total of 5998 boutons within the confines of the slice. At the light microscopic level, six putative sites of contact were identified on a synaptically coupled pyramidal cell (P1, Fig. 2*C*) and a similar number ($n = 4$) on a second, successively recorded

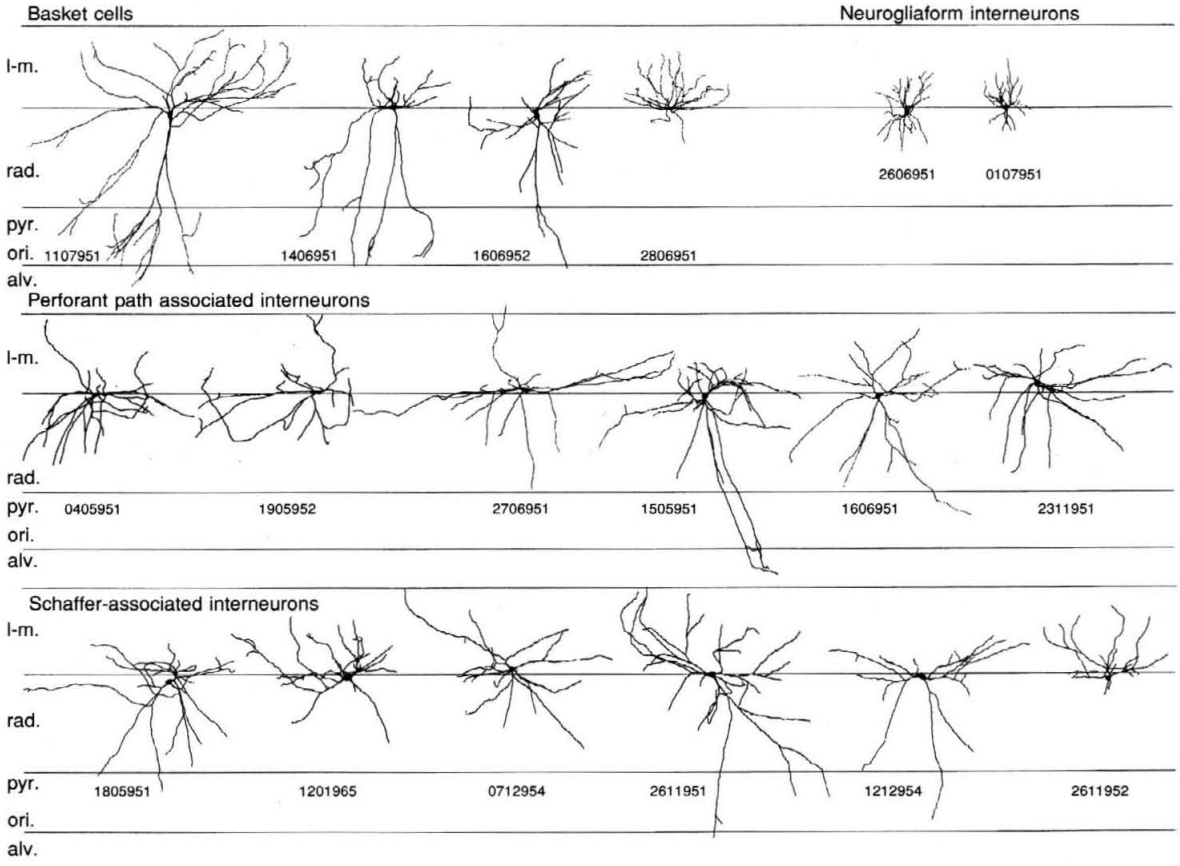

Figure 7. Dendritic geometry of interneurons at the stratum radiatum–stratum lacunosum-moleculare border

Based on their axonal distribution pattern (here not shown; for cells 2, 5, 6, 10 and 13 of Table 2, see Figs 1, 2, 3, 5 and 6, respectively), all cells could be incorporated into four major classes. Although differences in the axonal distribution pattern were generally more striking and sufficient for categorization, there appeared to be several group-specific distinguishing features in the dendritic architecture of stratum radiatum–stratum lacunosum-moleculare interneurons. Basket cell dendritic arbours (3/4) were radially elongated and spanned all hippocampal layers. Dendritic trees of Schaffer- and perforant path-associated interneurons had a more stellate appearance, with dendrites only infrequently entering stratum oriens (ori.) and the alveus (alv.). Both neurogliaform interneurons had very small stellate dendritic arbours. Abbreviations: l-m., stratum lacunosum-moleculare; rad., stratum radiatum; pyr., stratum pyramidale.

postsynaptic pyramidal cell (P3, contact sites not illustrated). All putative contacts were located on small calibre side branches of the apical dendrite, thus being in excellent correspondence with the electron microscopically determined random synaptic target profile for this cell (Table 2; Fig. 8*D*). Qualitatively and quantitatively similar observations were obtained for a second Schaffer-associated interneuron (Fig. 3*A* and *C*; 1201965; cell 6 of Table 2). The presynaptic axon established a total of six putative membrane appositions on the shaft of small calibre dendrites of the postsynaptic pyramidal cell (Fig. 3*C*), in agreement with the overall synaptic target profile for this cell (Table 2; Fig. 8*B* and *C*). Likewise, several additional members of this cell class were found to have either an exclusive or very high target preference for dendritic shafts (Table 2). Interestingly, however, in three instances (60% of cells examined) it was apparent that it was shafts of non-spiny dendrites which constituted up to 30% of postsynaptic targets, thus suggesting the divergent innervation of other hippocampal interneurons (Fig. 8*D*). Indeed, one of the Schaffer-associated interneurons (0706951) could be shown to elicit an IPSP in a concomitantly recorded pyramidal cell layer interneuron (data shown in Cobb *et al.* 1997). Hence these findings extend previous electron microscopic data (Kunkel, Lacaille & Schwartzkroin 1988), demonstrating that the output of light microscopically unclassified R–LM interneurons may be also directed towards non-pyramidal targets.

As for basket cells, there was a certain degree of heterogeneity in the morphology of Schaffer-associated interneurons (Figs 2*A*, 3*A* and 7). Some differences were noted with regard to the amount of axon entering stratum oriens, but also the adjoining subiculum (Fig. 3*A*). Dendritic arbours were generally stellate, with the majority of processes being contained within strata radiatum and lacunosum-moleculare. On occasion, however, marked dendritic anisotropies were noticeable or an individual dendrite could extend as far as the alveus (Fig. 7; cells 2611952 – cell 9 of Table 2 – and 2611951, respectively).

Perforant path-associated interneurons. These non-principal cells ($n = 6$) preferentially innervated stratum lacunosum-moleculare of the CA1 area (Fig. 5*A*), but across cells there was some degree of variability in the extent and density of axon. It was not uncommon for collaterals to cross the hippocampal fissure and ramify in the perforant path termination zone of the dentate gyrus ($n = 2$; Fig. 5*A*). Similar to Schaffer-associated cells, axon was also seen to invade the molecular layer of the subiculum ($n = 2$; Fig. 5*A*). Although relatively little axon of the perforant path-associated interneurons was contained in stratum radiatum, three of the cells had a few collaterals which descended to and arborized in stratum oriens (not shown). For the interneuron illustrated in Fig. 5*A* (0405951; cell 10 of Table 2) light microscopic counts indicated a total of 8015 axonal boutons, ~25% of which were located in the dentate gyrus and > 30% in the subiculum. An additional axon collateral was also noted to form a large terminal tuft within the prosubiculum (not shown). Thus this interneuron directed well in excess of 50% of its efferent output to three neighbouring hippocampal areas. Congruent with the axon of perforant path-associated neurons being distributed in dendritic layers, random electron microscopic bouton sampling revealed a high target preference for dendritic shafts and, to a lesser extent, for spines (Fig. 8*E–G*; Table 2). Interestingly, in one of the cells (2706951; cell 11 of Table 2) which exclusively targeted dendritic shafts, several of the synaptic junctions (30%) were situated at the origin of a dendritic spine receiving asymmetrical synaptic input (Fig. 8*F* and *G*, cell 11 of Table 2).

The dendrites of perforant path-associated interneurons were generally smooth and beaded. In contrast to basket cells, their dendritic arbours did not reveal any conspicuous polarities and/or tufts, with the majority of processes being contained within strata radiatum and lacunosum-moleculare (Fig. 7). Only one of the interneurons extended a small tuft of dendrites into the oriens/alveus border region, indicating the possibility of synaptic activation by recurrent pyramidal cell axons.

Neurogliaform interneurons. This type of interneuron was characterized by a small stellate dendritic arbour ($n = 2$; Figs 6*A* and 7). Moreover, neurogliaform cells had an extremely dense and, in terms of horizontal spread, compact axonal arbour which was contained within the strata radiatum and lacunosum-moleculare (Fig. 6*A*). When compared with other R–LM cells (Figs 1–3 and 5) the neurogliaform cell illustrated in Fig. 6*A* (2606951; cell 13 of Table 2) had a considerably smaller axonal arbour with a maximal proximo-distal extent not exceeding ~0·7 mm. Since no major axons had been truncated during the slicing procedure it is reasonable to assume that most of the axon was contained within the septo-temporal extent of the slice, thus suggesting an equally limited spread along the longitudinal hippocampal axis. Light microscopic counts yielded a total of 12959 boutons within the slice, 85% of which were located in stratum radiatum and the remaining 15% in stratum lacunosum-moleculare. The electron microscopic examination of randomly selected, vesicle-containing boutons revealed that neurogliaform interneurons predominantly target small-calibre dendritic shafts and, less frequently, spines (Fig. 8*H–J*; Table 2). It is noteworthy, however, that despite following a large number of boutons ($n = 60$) through strings of serial sections, only less than 50% ($n = 27$) could be shown to convincingly establish synaptic junctions (Fig. 8*H–J*; Table 2). To some extent, this may have been due to the small size and overall inconspicuousness of the synaptic junctions, although other factors such as the suboptimal ultrastructural preservation of the tissue cannot be excluded.

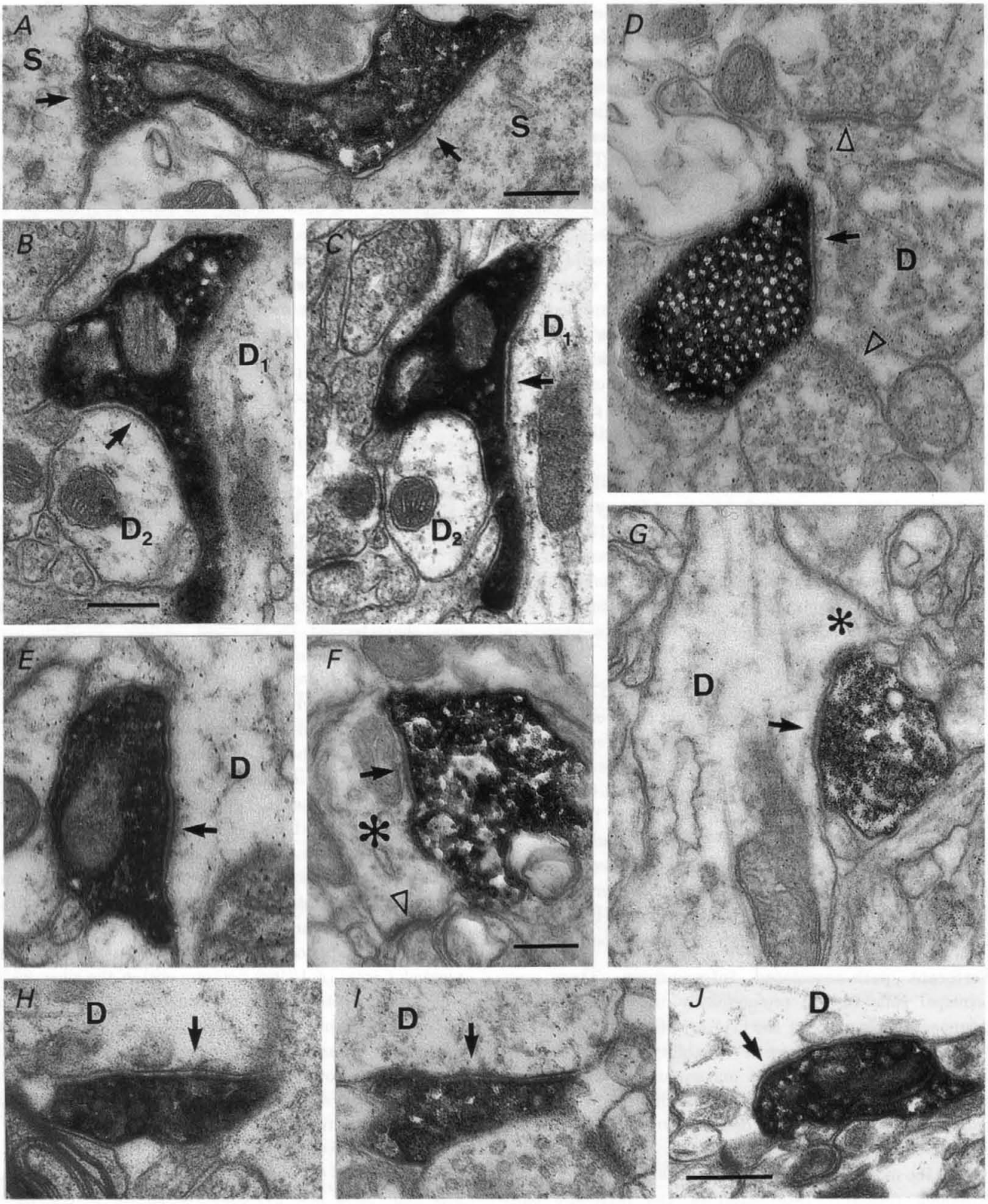

Figure 8. Electron micrographs of synaptic junctions established by identified interneurons at the stratum radiatum–stratum lacunosum-moleculare border

A–J, labelled boutons were followed through serial ultrathin sections until they formed synaptic junctions (arrows) with their respective postsynaptic targets (data shown in Table 2). *A*, basket cell (2806951; cell 4 of Table 2) bouton forming synaptic contacts (one each) with neighboring pyramidal somata (S). The rightmost synaptic junction is clearly identifiable, whereas the synaptic cleft of the junction shown to the left is

Unitary IPSPs evoked by R–LM interneurons in postsynaptic pyramidal cells

Paired intracellular recordings which were sufficiently stable to check for synaptic coupling were obtained in all anatomically recovered R–LM interneurons ($n = 22$). Thus, single or brief bursts of action potentials were elicited in the interneuron, while using on-line spike triggered averaging to monitor the response in a concomitantly recorded pyramidal cell ($n = 49$). Whenever necessary, a constant bias current was applied to hold the pyramidal neurons at a relatively depolarized membrane potential, on average $-58{\cdot}5 \pm 2{\cdot}8$ mV. In approximately one-third (19 of 49) of the recordings, activation of the interneuron elicited small-amplitude, short-latency (< 2 ms) unitary IPSPs (Figs 1*Bb* and *Bc*, 2*Bb–d*, 3*Bb* and *Bc*, 4*Aa*, *Ab*, *Ba* and *Bb*, and 6*Bb* and *Bc*). Interestingly, there was a rather dramatic cell type-specific difference in the incidence of synaptic coupling, with a success rate of > 80% in basket-to-pyramidal cell recordings (5 of 6), dropping to 65% (13 of 20) for Schaffer-associated interneuron-mediated effects, whereas it proved impossible to obtain convincing evidence for a unitary postsynaptic potential in all perforant path-associated interneuron-to-pyramidal cell somatic recordings (0 of 20). With regard to neurogliaform cell-mediated effects, three pyramidal neurons could be tested, and in one instance a postsynaptic effect was successfully recorded (Fig. 6*Bb* and *Bc*).

Regardless of whether they were evoked by brief trains or single action potentials, unitary R–LM interneuron-mediated IPSPs were rather small, ranging between 70 and 840 μV, with a mean amplitude of 263 ± 225 μV for single spike-evoked ($n = 6$; Table 1) and 304 ± 211 μV for the remainder of recordings where only summated responses were available ($n = 13$; Figs 2*Bc* and *Bd*, 3*Bc*, and 4*Bb*). In four instances (one basket and three Schaffer-associated cell-to-pyramidal pairs) averages of both single spike-evoked and summated postsynaptic responses were available. In an additional three cases, single action potentials of Schaffer-associated cells failed to elicit a measurable effect in a concomitantly recorded pyramidal neuron, although tetanic activation resulted in a sizable summated postsynaptic response. Prolonged firing of presynaptic R–LM interneurons ($n = 6$; all Schaffer-associated interneurons) with a burst of six to ten action potentials at frequencies of 70–100 Hz invariably lead to a substantial incremental increase of the summated response amplitude (Fig. 4*Ab* and *Bb*). Such summated IPSPs showed no appreciably prolonged duration and decayed back to baseline with a mean membrane time constant of 56 ± 19 ms (Fig. 4*Ab* and *Bb*).

Due to the nearly complete overlap of amplitude and noise distributions it was generally not feasible to determine the variability of individual, single action potential-evoked events. In one instance, however, a basket-to-pyramidal cell pair interaction, the signal-to-noise ratio was sufficiently favourable to warrant the construction of an amplitude histogram (1107951; cell 2 of Table 2; Fig. 1*C*). In this recording IPSPs were depolarizing events (Fig. 1*Bc*), since the postsynaptic pyramidal cell had been chloride loaded, with the extrapolated response reversal occurring at $-63{\cdot}5$ mV (Fig. 1*D*). Despite some degree of overlap with the noise distribution there appeared to be no prominent failure peak in the amplitude histogram, suggesting the overall paucity of postsynaptic response failures. Moreover, the variance of IPSP amplitudes was in a similar range to that of the noise measurements (0·081 and 0·052, respectively), suggesting a relatively reliable transmission with fairly constant strength. Following the procedure described by Miles & Wong (1984) the mean unitary IPSP conductance for this interaction was estimated to be 0·86 nS, thus being in the same range as those calculated for pyramidal cell layer basket-to-pyramidal cell pairs (Buhl *et al.* 1995).

Receptor pharmacology of R–LM interneuron-evoked unitary IPSPs

Although in many instances the small amplitudes of unitary events precluded reliable measurements, basket cell-evoked IPSPs appeared to have faster kinetics than those effects which were mediated by Schaffer-associated interneurons. However, despite the more prolonged kinetics of

more readily apparent after tilting the specimen (not shown). *B* and *C*, consecutive sections of a synaptic bouton of a Schaffer-associated interneuron (1201965; cell 6 of Table 2, shown in Fig. 3*A*). This terminal established two synaptic junctions with a large (D_1) and a small-calibre dendritic shaft (D_2). *D*, vesicle-filled terminal of a second Schaffer-associated interneuron (1805951; cell 5 of Table 2; shown in Fig. 2*A*) in synaptic contact with the shaft of a non-principal dendrite (D), also receiving converging synaptic input (arrowheads). *E*, a synaptic junction established by a perforant pathway-associated interneuron (1505951; cell 12 of Table 2) on a granule cell dendrite (D) in the outer molecular layer of the dentate gyrus. *F* and *G*, a second perforant pathway-associated interneuron (2706951; cell 11 of Table 2) formed synaptic junctions on medium to small-calibre dendritic shafts of pyramidal cells (D), here at the origin of spines (asterisks). The spine in *F* received a converging asymmetrical synapse (open triangle). *H–J*, randomly encountered synaptic junctions made by neurogliaform cells (*H* is cell 0107951, cell 14 of Table 2; *I* and *J* are cell 2606951, cell 13 of Table 2, see Fig. 6*A*). Neurogliaform cells formed rather inconspicuous synaptic junctions primarily within stratum radiatum (*H* and *J*) and, less commonly, in stratum lacunosum-moleculare (*I*). Scale bars: 0·25 μm. Bar in *A* also applies for *E* and *I*; bar in *B* also applies for *C*, *D* and *G*; bar in *F* also applies for *H*.

dendritically evoked IPSPs, their overall waveform was nevertheless more reminiscent of a $GABA_A$ receptor-mediated chloride conductance. Furthermore, this notion is also strengthened by the fact that the calculated reversal potentials for those IPSPs which were mediated by Schaffer-associated interneurons ($-70{\cdot}2 \pm 1{\cdot}0$ mV; $n = 3$) were in the same range as the chloride equilibrium potential.

We then proceeded to using bath-applied amino acid receptor antagonists to further elucidate the receptor mechanisms underlying R–LM interneuron-mediated IPSPs ($n = 5$; 1 basket-to-pyramidal cell pair, 4 Schaffer-associated interneuron effects). In all instances, mean amplitudes of unitary IPSPs remained unchanged in the presence of 10 μM CNQX and 50 μM AP5 (Fig. 3*Bc*), demonstrating that the effects were neither di- or polysynaptically mediated, involving a glutamatergic synapse. Subsequent superfusion with 10 μM bicuculline hydrochloride nearly abolished the responses (96 ± 10% reduction, Figs 1*Bd* and 3*Bd*), indicating that most of the measurable response was due to the activation of either somatically, as in the case for basket cells, or dendritically located $GABA_A$ receptors.

DISCUSSION

Correlated light and electron microscopy of intracellularly labelled hippocampal R–LM interneurons revealed four distinct populations of non-principal neurons, showing prominent differences with regard to the domain-specific GABAergic innervation of principal neurons. Employing paired intracellular recordings, three classes of R–LM neurons could be shown to elicit short-latency IPSPs in concomitantly recorded pyramidal cells. Unitary IPSPs evoked by basket and Schaffer-associated neurons could be abolished by a competitive $GABA_A$ receptor antagonist. We have thus classified and characterized several populations of hippocampal interneurons. These data extend the complexity of GABAergic pyramidal cell innervation and their functional implications will be considered below.

Identity of R–LM interneurons

Although R–LM basket cells densely innervate the pyramidal cell layer and direct their output selectively to the perisomatic domain of their postsynaptic targets, it is nevertheless unlikely that they belong to the parvalbumin-containing class of basket cells, since in the CA1 area the latter are almost exclusively concentrated within the pyramidal cell layer and throughout stratum oriens (Kosaka, Katsumaru, Hama, Wu & Heizmann, 1987). In contrast basket cells which are immunoreactive for the peptide cholecystokinin (CCK) are considerably more abundant at the R–LM border (Nunzi, Gorio, Milan, Freund, Somogyi & Smith, 1985) and a wealth of recent data on the colocalization of calcium-binding proteins and neuropeptide co-transmitters strongly suggests that parvalbumin- and CCK-containing neurons form two distinct, non-overlapping populations of basket cells (reviewed in Freund & Buzsáki, 1996).

Non-principal neurons with a morphology similar to that of Schaffer-associated cells have been described previously (Kawaguchi & Hama, 1988; Lacaille & Schwartzkroin, 1988*a*; Williams *et al.* 1994), although a detailed comparison is hampered either by the lack of detailed reconstructions or less extensively labelled axonal arbours. With regard to their axonal distribution and efferent target profile Schaffer-associated neurons closely resemble the class of dendrite-targeting bistratified cells (Buhl *et al.* 1994; Halasy *et al.* 1996) and may also contain the calcium-binding protein calbindin (Sík, Penttonen, Ylinen & Buzsáki, 1995). Marked differences are, however, apparent in the dendritic geometry of these neurons. Bistratified cells have few, if any, of their dendrites in stratum lacunosum-moleculare (Halasy *et al.* 1996), whereas those of Schaffer-associated interneurons are abundant in this layer, indicating a stronger activation by entorhinal input and perhaps also by afferents from the nucleus reuniens thalami (Wouterlood, Saldana & Witter, 1990).

Amongst R–LM neurons, perforant path-associated cells were particularly striking due to the intimate association of their axonal arbours with a major set of hippocampal afferents, even extending across boundaries, such as the hippocampal fissure, into adjoining subfields. A similar degree of specificity has been also noted for the presumably somatostatin-containing class of hilar perforant pathway-associated (HIPP) cells in the dentate gyrus (Han *et al.* 1993). However, although the axons of HIPP cells and their somatostatin-containing counterparts in the other hippocampal subfields also co-laminate with entorhinal afferents, their dendritic architecture predisposes them to receive recurrent excitatory input (Gulyás *et al.* 1993; Han *et al.* 1993; Maccaferri & McBain, 1995). In contrast, perforant path-associated cells in the CA1 area had most of their dendrites confined to strata radiatum and lacunosum-moleculare, suggesting a more prominent role in feedforward activation and therefore more closely resembling molecular layer perforant pathway-associated (MOPP) cells in the dentate gyrus (Han *et al.* 1993; Halasy & Somogyi, 1993).

Despite the limited sample size it appeared justified to incorporate neurogliaform cells into a separate category, owing to their highly distinct morphology. Moreover, a recently published single example of an intracellularly labelled R–LM interneuron corresponds very closely to our cells (Khazipov, Congar & Ben-Ari, 1995). In contrast to the other hippocampal categories of dendrite-targeting cells, the axon of neurogliaform interneurons could not be easily reconciled with the laminar distribution of any of the major excitatory pathways, and is thus not unlike interneurons in the dentate gyrus which have been shown to innervate the

entire molecular layer (Soriano & Frotscher, 1993). Although neurogliaform cells may not possess a significant degree of laminar specificity, it is conceivable that their small dimensions predispose them to form an association with subsets of proximo-distally aligned extrinsic afferents, reflecting the orderly topography of associational as well as entorhinal inputs to the CA1 area (Amaral & Witter, 1989).

Synaptic and receptor mechanisms of R–LM interneuron-mediated IPSPs

Consistent with earlier data describing the postsynaptic effect and receptor mechanisms of morphologically unidentified R–LM interneurons (Lacaille & Schwartzkroin, 1988*b*; Ouardouz & Lacaille, 1997) we have now shown three distinct classes of such non-principal cells to evoke short-latency monosynaptic IPSPs. In order to maximize the extent of labelling and the degree of ultrastructural preservation, sharp microelectrode recordings in conventional thick slices were employed. Due to the limitations of this approach, amplitudes of single unitary events were generally below detection threshold. Moreover, despite using on-line averaging techniques, it was often necessary to elicit a brief burst of three to seven presynaptic action potentials to check for synaptic coupling. When employing this activation paradigm, the postsynaptic effect elicited by R–LM interneurons invariably showed a substantial degree of response summation which appeared to be rather prominent in the class of Schaffer-associated cells. Therefore, temporal coding (e.g. burst *vs.* single volley) of afferent information may result in prominent differences of the postsynaptic response duration and magnitude. The association with the innervation from the CA3 area may be of particular relevance, since CA3 pyramidal neurons show state-dependent changes in their activity/discharge pattern. Thus, single activation of Schaffer-associated interneurons will result in a small postsynaptic effect, whereas more efficacious, summated IPSPs may be associated with CA3 population bursts during sharp waves (Buzsáki, 1989).

In addition to pyramidal cell layer basket and axo-axonic cells (Buhl *et al.* 1994), R–LM basket and dendrite-targeting Schaffer-associated cells have now been shown to evoke fast, $GABA_A$ receptor-mediated IPSPs, thus being in accordance with the immunocytochemically determined distribution of synaptic $GABA_A$ receptor proteins (Nusser, Sieghart, Benke, Fritschy & Somogyi, 1996). Qualitatively similar findings, both with regard to the kinetics and/or receptor mechanism of unitary IPSPs evoked by hippocampal interneurons have been reported (Knowles & Schwartzkroin, 1981; Miles & Wong, 1984; Scharfman, Kunkel & Schwartzkroin, 1990; Miles, Tóth, Gulyás, Hájos & Freund, 1996; Ouardouz & Lacaille, 1997) Hence, the source of $GABA_B$ receptor-mediated synaptic potentials which can be readily evoked following the synaptic or direct stimulation of interneurons remains to be determined (Thompson, 1994). At present, several classes of interneurons remain for which the postsynaptic receptor mechanisms are unknown, amongst them the classes of perforant path-associated cells. Alternatively, if $GABA_B$ receptors were, as with metabotropic glutamate receptors (Baude, Nusser, Roberts, Mulvihil, McIlhinney & Somogyi, 1993), located either peri- or extrasynaptically it is conceivable that the tetanic activation of a single or the concomitant stimulation of several presynaptic interneurons is a prerequisite for their activation. Our own data would rather support the latter scenario, since repetitive activation of single R–LM interneurons did not result in unitary effects with decay kinetics which were compatible with those reported for $GABA_B$ receptor-mediated events (Otis, DeKoninck & Mody, 1993). Moreover, this notion is also supported by findings indicating that $GABA_B$ receptor-mediated use-dependent presynaptic depression at inhibitory hippocampal synapses requires the conjoint activation of several inhibitory neurons (Lambert & Wilson, 1994).

The heterogeneity of R–LM interneurons is indicative of their functional diversity

Subdividing the neuronal surface by segregated or partially overlapping GABAergic inputs provides a versatile machinery for segregating output regulation and dendritic integration. Thus, interneurons which target the perisomatic region have been shown to synchronize principal cell activity by interacting with intrinsic membrane potential oscillations (Cobb, Buhl, Halasy, Paulsen & Somogyi, 1995). Regarding their efferent connectivity, R–LM basket cells may therefore subserve a similar functional role, but their dendritic geometry indicates that they are driven more strongly by entorhinal afferents than stratum pyramidale basket cells (Halasy *et al.* 1996). Conversely, IPSPs generated by R–LM dendrite-targeting cells may be effective in shunting excitatory conductances (Staley & Mody, 1992) or by exerting a presynaptic action due to the pathway selective activation of $GABA_B$ receptors on neighbouring glutamatergic terminals (Isaacson, Solis & Nicoll, 1993). In addition, more dynamic roles can be envisaged for effects mediated by dendrite-targeting interneurons, such as interactions with voltage-gated conductances to either control the generation of dendritic calcium spikes (Miles *et al.* 1996) or the back-propagation of action potentials (Spruston, Schiller, Stuart & Sakmann, 1995). Finally, appropriately timed dendritic IPSPs may specifically curtail the decay of excitatory events and thus narrow the window for their temporal summation (Softky, 1994).

Similar to R–LM basket cells, dendrite-targeting interneurons at the R–LM border have a large fraction of their dendrites in the entorhinal termination zone, but their dendritic architecture also predisposes them to receiving a substantial input from the CA3 area. As a consequence of this dual innervation, R–LM border cells are therefore well suited to establish a GABAergic cross-influence between the

two major excitatory pathways, with the entorhinal activation of Schaffer-associated neurons modulating input from the CA3 area and vice versa. Therefore, the domain-specific innervation by different sets of R–LM interneurons may not only be suitable to shift the balance of inhibition between different membrane compartments (Acsády *et al.* 1996), but also to focus and amplify signals from the entorhinal cortex, as has been postulated from *in vivo* experiments in the dentate gyrus (Moser, 1996).

Acsády, L., Görcs, T. J. & Freund, T. F. (1996). Different populations of vasoactive intestinal polypeptide-immunoreactive interneurons are specialized to control pyramidal cells or interneurons in the hippocampus. *Neuroscience* **73**, 317–334.

Amaral, D. G. & Witter, M. P. (1989). The three-dimensional organization of the hippocampal formation: a review of anatomical data. *Neuroscience* **31**, 571–591.

Baude, A., Nusser, Z., Roberts, J. D. B., Mulvihill, E., McIlhinney, R. A. J. & Somogyi, P. (1993). The metabotropic glutamate receptor (mGluR1α) is concentrated at perisynaptic membrane of neuronal subpopulations as detected by immunogold reaction. *Neuron* **11**, 771–787.

Buhl, E. H., Cobb, S. R., Halasy, K. & Somogyi, P. (1995). Properties of unitary IPSPs evoked by anatomically identified basket cells in the rat hippocampus. *European Journal of Neuroscience* **7**, 1989–2004.

Buhl, E. H., Halasy, K. & Somogyi, P. (1994). Diverse sources of hippocampal unitary inhibitory postsynaptic potentials and the number of synaptic release sites. *Nature* **368**, 823–828.

Buhl, E. H., Szilágyi, T., Halasy, K. & Somogyi, P. (1996). Physiological properties of anatomically identified basket and bistratified cells in the CA1 area of the rat hippocampus in vitro. *Hippocampus* **6**, 294–305.

Buzsáki, G. (1989). Two-stage model of memory trace formation: a role for 'noisy' brain states. *Neuroscience* **31**, 551–570.

Cobb, S. R., Buhl, E. H., Halasy, K., Paulsen, O. & Somogyi, P. (1995). Synchronization of neuronal activity in hippocampus by individual GABAergic interneurons. *Nature* **378**, 75–78.

Cobb, S. R., Halasy, K., Vida, I., Nyíri, G., Tamás, G., Buhl, E. H. & Somogyi, P. (1997). Synaptic effects of identified interneurones innervating both interneurons and pyramidal cells in the rat hippocampus. *Neuroscience* **79**, 629–648.

Freund, T. F. & Buzsáki, G. (1996). Interneurons of the hippocampus. *Hippocampus* **6**, 347–470.

Gulyás, A. I., Hájos, N. & Freund, T. F. (1996). Interneurons containing calretinin are specialized to control other interneurons in the rat hippocampus. *Journal of Neuroscience* **16**, 3397–3411.

Gulyás, A. I., Miles, R., Hájos, N. & Freund, T. F. (1993). Precision and variability in postsynaptic target selection of inhibitory cells in the hippocampal CA3 region. *European Journal of Neuroscience* **5**, 1729–1751.

Halasy, K., Buhl, E. H., Lörinczi, Z., Tamás, G. & Somogyi, P. (1996). Synaptic target selectivity and input of GABAergic basket and bistratified interneurons in the CA1 area of the rat hippocampus. *Hippocampus* **6**, 306–329.

Halasy, K. & Somogyi, P. (1993). Subdivisions in the multiple GABAergic innervation of granule cells in the dentate gyrus of the rat hippocampus *European Journal of Neuroscience* **5**, 411–429.

Han, Z.-S., Buhl, E. H., Lörinczi, Z. & Somogyi, P. (1993). A high degree of spatial selectivity in the axonal and dendritic domains of physiologically identified local-circuit neurons in the dentate gyrus of the rat hippocampus. *European Journal of Neuroscience* **5**, 395–410.

Isaacson, J. S., Solis, J. M. & Nicoll, R. A. (1993). Local and diffuse synaptic actions of GABA in the hippocampus. *Neuron* **10**, 165–175.

Kawaguchi, Y. & Hama, K. (1988). Physiological heterogeneity of nonpyramidal cells in rat hippocampal CA1 region. *Experimental Brain Research* **72**, 494–502.

Khazipov, R., Congar, P. & Ben-Ari, Y. (1995). Hippocampal CA1 lacunosum-moleculare interneurons: modulation of monosynaptic GABAergic IPSCs by presynaptic $GABA_B$ receptors. *Journal of Neurophysiology* **74**, 2126–2137.

Knowles, W. D. & Schwartzkroin, P. A. (1981). Local circuit synaptic interactions in hippocampal brain slices. *Journal of Neuroscience* **1**, 318–322.

Kosaka, T., Katsumaru, H., Hama, K., Wu, J.-Y. & Heizmann, C. W. (1987). GABAergic neurons containing the Ca^{2+}-binding protein parvalbumin in the rat hippocampus and dentate gyrus. *Brain Research* **419**, 119–130.

Kunkel, D. D., Lacaille, J.-C. & Schwartzkroin, P. A. (1988). Ultrastructure of stratum lacunosum-moleculare interneurons of hippocampal CA1 region. *Synapse* **2**, 382–394.

Lacaille, J.-C. & Schwartzkroin, P. A. (1988*a*). Stratum lacunosum-moleculare interneurons of hippocampal CA1 region. I. Intracellular response characteristics, synaptic responses, and morphology. *Journal of Neuroscience* **8**, 1400–1410.

Lacaille, J.-C. & Schwartzkroin, P. A. (1988*b*). Stratum lacunosum-moleculare interneurons of hippocampal CA1 region. II. Intrasomatic and intradendritic recordings of local circuit synaptic interactions. *Journal of Neuroscience* **8**, 1411–1424.

Lambert, N. A. & Wilson, W. A. (1994). Temporally distinct mechanisms of use-dependent depression at inhibitory synapses in the rat hippocampus *in vitro*. *Journal of Neurophysiology* **72**, 121–130.

Maccaferri, G. & McBain, C. J. (1995). Passive propagation of LTD to stratum oriens-alveus inhibitory neurons modulates the temporoammonic input to the hippocampal CA1 region. *Neuron* **15**, 137–145.

Miles, R., Tóth, K., Gulyás, A. I., Hájos, N. & Freund, T. F. (1996). Differences between somatic and dendritic inhibition in the hippocampus. *Neuron* **16**, 815–823.

Miles, R. & Wong, R. K. S. (1984). Unitary inhibitory synaptic potentials in the guinea-pig hippocampus *in vitro*. *Journal of Physiology* **356**, 97–113.

Misgeld, U., Bijak, M. & Jarolimek, W. (1995). A physiological role for $GABA_B$ receptors and the effects of baclofen in the mammalian central nervous system. *Progress in Neurobiology* **46**, 423–462.

Mody, I., De Koninck, Y., Otis, T. S. & Soltesz, I. (1994). Bridging the cleft at GABA synapses in the brain. *Trends in Neurosciences* **17**, 517–525.

Moser, E. I. (1996). Altered inhibition of dentate granule cells during spatial learning in an exploration task. *Journal of Neuroscience* **16**, 1247–1259.

NUNZI, M. G., GORIO, A., MILAN, F., FREUND, T. F., SOMOGYI, P. & SMITH, A. D. (1985). Cholecystokinin-immunoreactive cells form symmetrical synaptic contacts with pyramidal and nonpyramidal neurons in the hippocampus. *Journal of Comparative Neurology* **237**, 485–505.

NUSSER, Z., SIEGHART, W., BENKE, D., FRITSCHY, J.-M. & SOMOGYI, P. (1996). Differential synaptic localization of two major γ-aminobutyric acid type A receptor α subunits on hippocampal pyramidal cells. *Proceedings of the National Academy of Sciences of the USA* **93**, 11939–11944.

OTIS, T. S., DE KONINCK, Y. & MODY, I. (1993). Characterization of synaptically elicited $GABA_B$ responses using patch-clamp recordings in rat hippocampal slices. *Journal of Physiology* **463**, 391–407.

OUARDOUZ, M. & LACAILLE, J. C. (1997). Properties of unitary IPSCs in hippocampal pyramidal cells originating from different types of interneurons in young rats. *Journal of Neurophysiology* **77**, 1939–1949.

SCHARFMAN, H. E., KUNKEL, D. D. & SCHWARTZKROIN, P. A. (1990). Synaptic connections of dentate granule cells and hilar neurons: results of paired intracellular recordings and intracellular horseradish peroxidase injections. *Neuroscience* **37**, 693–707.

SÍK, A., PENTTONEN, M., YLINEN, A. M. & BUZSÁKI, G. (1995). Hippocampal CA1 interneurons: an *in vivo* intracellular labeling study. *Journal of Neuroscience* **15**, 6651–6665.

SOFTKY, W. (1994). Sub-millisecond coincidence detection in active dendritic trees. *Neuroscience* **58**, 13–41.

SOLIS, J. M. & NICOLL, R. A. (1992). Postsynaptic action of endogenous GABA released by nipecotic acid in the hippocampus. *Neuroscience Letters* **147**, 16–20.

SOMOGYI, P., FREUND, T. F., HODGSON, A. J., SOMOGYI, J., BEROUKAS, D. & CHUBB, I. W. (1985). Identified axo-axonic cells are immunoreactive for GABA in the hippocampus and visual cortex of the cat. *Brain Research* **332**, 143–149.

SORIANO, E. & FROTSCHER, M. (1993). GABAergic innervation of the rat fascia dentata: a novel type of interneuron in the granule cell layer with extensive axonal arborization in the molecular layer. *Journal of Comparative Neurology* **334**, 385–396.

SPRUSTON, N., SCHILLER, Y., STUART, G. & SAKMANN, B. (1995). Activity-dependent action potential invasion and calcium influx into hippocampal CA1 dendrites. *Science* **268**, 297–300.

STALEY, K. J. & MODY, I. (1992). Shunting of excitatory input to dentate gyrus granule cells by a depolarizing $GABA_A$ receptor-mediated postsynaptic conductance. *Journal of Neurophysiology* **68**, 197–212.

SZENTÁGOTHAI, J. (1973). Synaptology of the visual cortex. In *Handbook of Sensory Physiology*, ed. JUNG, R., AUTRUM, H., LOEWENSTEIN, W. R., MCKAY, D. M. & TENBER, H. L., pp. 269–324. Springer, Berlin.

THOMPSON, S. M. (1994). Modulation of inhibitory synaptic transmission in the hippocampus. *Progress in Neurobiology* **42**, 575–609.

THOMPSON, S. M. & GÄHWILER, B. H. (1992). Effects of the GABA uptake inhibitor tiagabine on inhibitory synaptic potentials in rat hippocampal slice cultures. *Journal of Neurophysiology* **67**, 1698–1701.

WILLIAMS, S. & LACAILLE, J.-C. (1992). $GABA_B$ receptor-mediated inhibitory postsynaptic potentials evoked by electrical stimulation and by glutamate stimulation of interneurons in stratum lacunosum-moleculare in hippocampal CA1 pyramidal cells *in vitro*. *Synapse* **11**, 249–258.

WILLIAMS, S., SAMULACK, D. D., BEAULIEU, C. & LACAILLE, J.-C. (1994). Membrane properties and synaptic responses of interneurons located near the stratum lacunosum-moleculare/radiatum border of area CA1 in whole-cell recordings from rat hippocampal slices. *Journal of Neurophysiology* **71**, 2217–2235.

WOUTERLOOD, F. G., SALDANA, E. & WITTER, M. P. (1990). Projection from the nucleus reuniens thalami to the hippocampal region: light and electron microscopic tracing study in the rat with the anterograde tracer *Phaseolus vulgaris*-leucoagglutinin. *Journal of Comparative Neurology* **296**, 179–203.

Acknowledgements

We are grateful to Mr P. Jays and Mr F. D. Kennedy for photographic assistance. This work was funded in part by EC Grant BIO4-CT96-0585 and the Wellcome Trust. I.V. was supported by the Hungarian National Research Found (OTKA W015001 and T020567). C.S. received a Soros Visiting Studentship. E.H.B. also holds a Medical Research Fellowship at Corpus Christi College, Oxford.

Corresponding author

E. H. Buhl: MRC Anatomical Neuropharmacology Unit, Department of Pharmacology, Oxford University, Oxford OX1 3TH, UK

Email: eberhard.buhl@pharmacology.oxford.ac.uk

Author's present address

Imre Vida: Department of Anatomy, University of Freiburg, 79001 Freiburg, Germany.